Bubble Wake Interaction with Convective flow from a heated vertical flat plate.

Y.M.C. Delauré, V.S.S. Chan and D.B. Murray
Department of Mechanical and Manufacturing Engineering,
Trinity College, Dublin 2, Ireland.

ABSTRACT

Time-synchronised flow velocity, temperature, and heat flux measurements were preformed to characterise the interaction of a single rising ellipsoidal bubble with the free convection flow from a heated vertical flat surface. The heat transfer measurements from the surface were provided by a hot film heat flux sensor calibrated using a pre-calibrated microfoil heat flux sensor. Two thermocouples were used to measure the temperature difference between the solid surface and the adjacent fluid layer and the velocity flow was mapped by a time-resolved digital particle image velocimetry technique (DPIV). Heat flux fluctuations, preceding and following the bubble passage, were shown to correlate with variation in both local flow velocities and fluid temperatures. The bubble induced swirling flow was shown, for example, either to assist or to hinder the heat transfer process by assisting or opposing the free convection flow (see velocity plot below). Vortices, shed by the free rising bubble and convected within its wake, were also linked to the transport of colder fluid into contact with the heated surface. When both flow and temperature effects combined to enhance the convective cooling process a magnification larger than 5 was measured from the sample test selected for the present analysis, while the bubble effect was shown to last beyond the 4.4s duration of the test records.

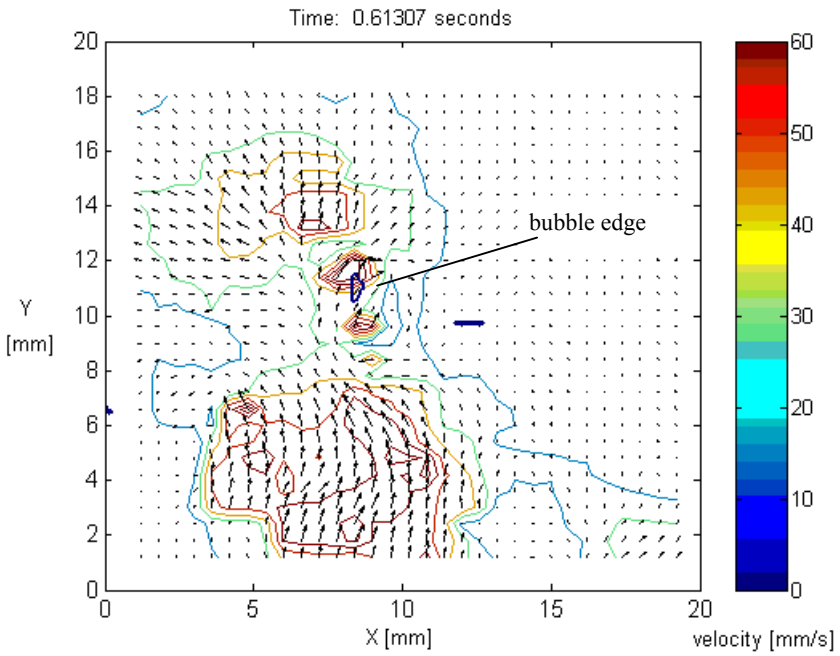

Flow velocity plots from PIV measurements shown with scaled velocity vectors, velocity contour plots showing velocity amplitude in mm/s, a contour plot of the right hand side of the bubble interface and a straight line indicating the hot film position and dimension.

1 INTRODUCTION

Nucleate pool boiling, which is of engineering significance for such areas as internal combustion engine block cooling, pressurised water nuclear reactors and heat exchangers, has been studied extensively by engineers and scientists. The associated high rate of heat transfer effect is known to result from phase change on heated surfaces as well as from convective cooling due to bubble detachment and agitation. The numerical model developed by Yoon et al. (2001) suggests, for example, that the mixing due to a single detaching vapour bubble can contribute up to 80% of the total heat flux from a horizontal surface heated at 110 ºC in subcooled water. An earlier experimental study by Forster and Grief (1959) also concluded that the high rate of heat transfer associated with nucleate boiling was largely caused by the convective action of the rising bubbles. In the case of injected steam bubbles sliding upward along inclined flat plates, heated at 104°C in water maintained at 96°C, Yan et al. (1997) showed how an evaporative cooling process occurred first as the bubble slides above the block. Evaporation is then caused by conduction through the thin fluid film separating the steam bubble from the heated surface. Convective cooling was suggested to occur in a second stage as the bubble wake reaches the heated surface. Although the study investigated in detail description of the effect of the bubble passage on temperature changes at the solid surface, it is felt that a more in-depth understanding of the cooling processes considered would have required a descriptions of the dynamics of the bubble and its wake and their interaction with the free convection flow from the surface.

The present experimental study aimed at providing information on local flow patterns and temperature gradients in order to characterise the effect of the sliding bubble on the local heat transfer in an otherwise similar set-up to that considered by Yan et al. (1997). The study, however, focused on convective cooling effects of single bubbles by ensuring that evaporation did not occur. Air bubbles instead of steam were injected below a heated copper block immersed in water and allowed to impact and slide along the block surface. The instrumentation of the block surface included two thermocouples and a hot film sensor to characterise the local heat transfer from the block surface to the fluid layer. The flow velocity field was mapped over a 19.5mm square plane centred over the hot film using a Digital Particle Image Velocimetry (DPIV) technique. The corresponding experimental set-up and procedure are presented in the two first parts. Sample results obtained with one bubble and a vertical block are then discussed to illustrate the main flow and heat transfer processes involved.

2 EXPERIMENTAL METHODS AND PROCEDURES

2.1 Experimental set-up

Local flow conditions including velocity and temperature gradients need to be measured simultaneously with the heat transfer from the surface to achieve a detailed investigation of the convective cooling process due to a bubble passage. A series of trial tests were conducted at the onset of the project to clarify the experimental requirements. Particle Image Velocimetry (PIV) emerged as the optimal non-intrusive optical technique for flow velocity mapping whereas local heat transfer and temperature measurements required direct instrumentation of the heated surface. The corresponding experimental set-up is outlined below:

(i) A copper block 100mm high, 50mm wide and 25mm deep was designed to provide the heated flat test surface and was machined with two internal cylindrical holes to house a pair of 535W cartridge heaters. The block/heater arrangement was carefully designed to minimise heterogeneity in the heat flux distribution over the block surface.

(ii) The volume of the tank had to be sufficiently large to ensure that the water bulk temperature be maintained relatively constant over a test series duration of about 15 minutes. Attenuation of a laser light sheet used for DPIV as it propagates through the tank walls and the water column also needed to be minimised. These requirements led to the design of a relatively narrow tank 780mm high with a base 230mm by 230mm and constructed with 6mm thick glass panes.

(iii) A 300mW Argon Ion Laser was incorporated to provide the continuous light source for the purpose of PIV tests, while 50µm Polyamid Particles of 1.03 g/cm^3 density were used for seeding.

(iv) The high speed imaging system adapted to complete the PIV test rig is based on three components:
   a. a digital CCD high-speed camera (Dalsa CA-D6-0256) capable of acquiring images at a frame rate of up to 997Hz at a spatial resolution of 260pixels x 260pixels.
   b. memory buffers and interfacing boards required by the high frame rate and hence high throughput of the camera.
   c. the acquisition and process units based on the 'Video Savant' commercial software previously customised to allow triggering of data acquisition simultaneously with other instruments.

(v) The bubble injection system designed and built, purposely, is composed of an air chamber and a cylindrical release system. The rectangular air chamber is immersed at the bottom of the tank and connected to an external syringe by a flexible hose via the bottom panel. A 0.8mm hole drilled through the top section of the air chamber allows small air bubbles to be injected into the tank. These bubbles are, in turn, used to fill either of two cavities drilled on the surface of the cylindrical block held directly above. The size of the cavity controls the bubble size while the selection of the cavity and the release of the bubble are achieved by rotating the block. The block's cylindrical shape ensures that disturbance of the flow is minimised, while the two-step release approach was needed to delay the bubble release until stable flow conditions were reached in case excess air was injected by the syringe.

(vi) The copper block itself was instrumented with two heat flux sensors aligned 57mm from the bottom edge of the block along with one thermocouple embedded within the block. The heat flux sensors used are (i) a 0.1mm thick microfoil sensor consisting of three thin layers of Kapton insulating material and T type thermopiles and (ii) a 0.1mm thick hotfilm sensor composed of a 0.1mm wide and 1.5mm long Nickel film deposited on a 50μm thick polyimide layer and coated with a 50μm thick polyimide layer. The hot film is mounted perpendicular to the main flow direction, ie horizontally while the microfoil sensor is positioned with the thermopiles at the same distance from the block bottom and side edges as the hot film. 0.3mm deep flat depressions were machined into the block surface to accommodate the two heat flux sensors and an additional 0.1mm thick layer of double sided adhesive tape used to glue the heat flux sensors on the block surface. An extra 0.1mm depth of machining was included to ensure that the silicon layer spread along the edges of the sensors to ensure adequate sealing, would not bulge out of the block surface plane. The resulting 100μm depression on the block surface should, however, have a negligible impact on the laminar flow, which is measured, in this case, 3mm from the block surface. A 1.5mm wide and 0.7mm thick groove was also machined below the hot film sensor to accommodate the internal thermocouple wires. The groove was slightly offset from the horizontal position of the hot film to minimise the alteration of the block structure below the measurement point. The thermocouple junction was, however, positioned directly against the edge of the groove as close as possible to hot film to measure the temperature of the block surface below the hot film. The groove was finally filled with thermally conductive adhesive (conductivity coefficient of 0.82W/mK) filling the air gaps left between the block and the sensor. An additional thermocouple was fixed just above and to the left of the hot film (taking the direction of free convection flow as reference) to provide a temperature reading within the fluid domain. The thermocouple junction and the connection wires were glued externally and protrude, from the surface, by 0.7mm. Finally a third external thermocouple was inserted into the tank to record the bulk water temperature at the level of the bottom edge of the block in its vertical position. A more detailed description of the block configuration and instrumentation is shown on Figure 1.

(vii) Data acquisition from the two thermocouples and two heat flux sensors is performed by an external 14-bit Analogue to Digital Converter (ADC) connected to a PCI card. The ADC controller includes optional 40kHz analogue filters, which were selected on all channels as high frequency noise was found to generate random fluctuation due to aliasing. The thermocouples are connected directly to the external converter, which includes optional cold junction compensations on each channel. A 1000X gain is applied to the output from the microfoil sensor (calibrated at $0.0532728\mu V/Wm^{-2}$) by means of an external analogue amplifier, to increase the relative output voltage range for optimal resolution of the analogue to digital conversion within the 0 to 80mV range selected for this device. The Constant Temperature Anenometer (CTA) bridge (Mini CTA 54T30 from Dantec) used to control the hotfilm sensor has a signal output ranging from 0 to 5Volts, which can be read directly by the ADC controller. Acquisition was triggered by an external pulse generator with a delay of the order of 5 to 25μs, each channel being sampled sequentially at 6μs intervals. All measurements were performed by differential input using the common rejection mode.

Although the present study focuses on the particular case of a vertical surface, the test rig was designed to allow the block to be inclined from 0° (vertical position) to 90°. The complete experimental set-up, with an inclined block configuration, is illustrated in Figure 2.

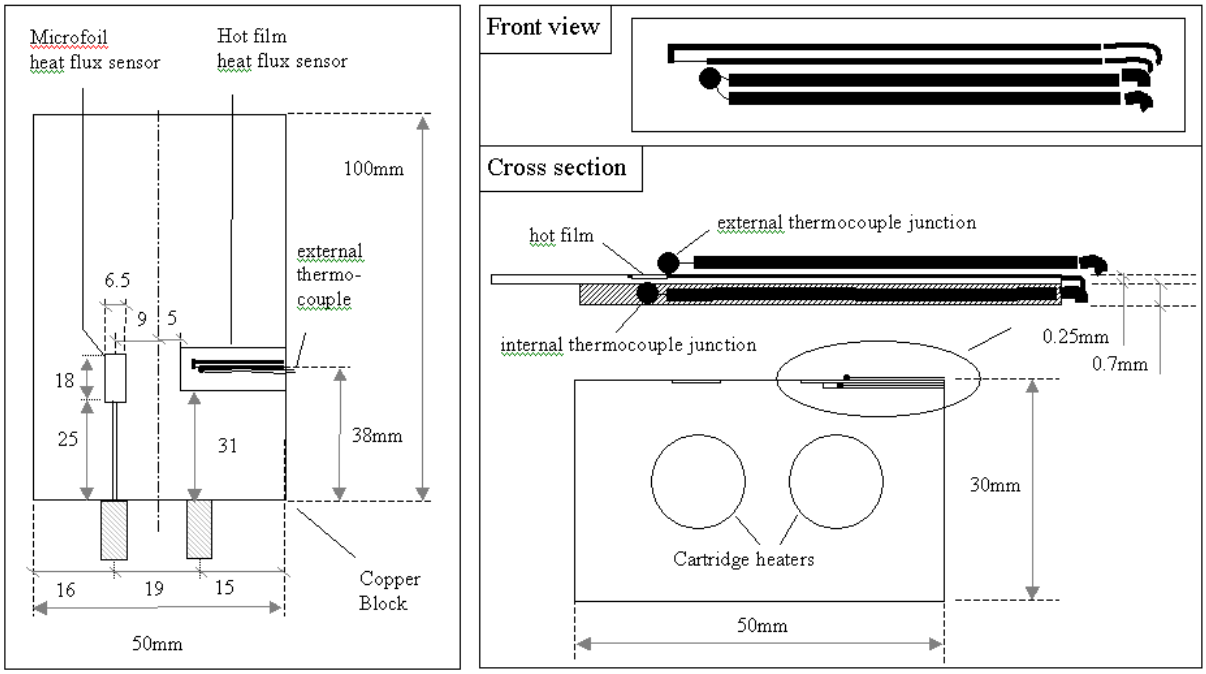

Figure 1 Diagram of block and instrumentation. Left: Front view of instrumented side of block showing the two heat flux sensors and the external thermocouple – not to scale. Bottom right : cross section of block along hot film with blown-up view of hot film sensor including external and internal thermocouples - lower part to scale. Top right: Blow-up front view of hot film sensor including underlying internal thermocouple.

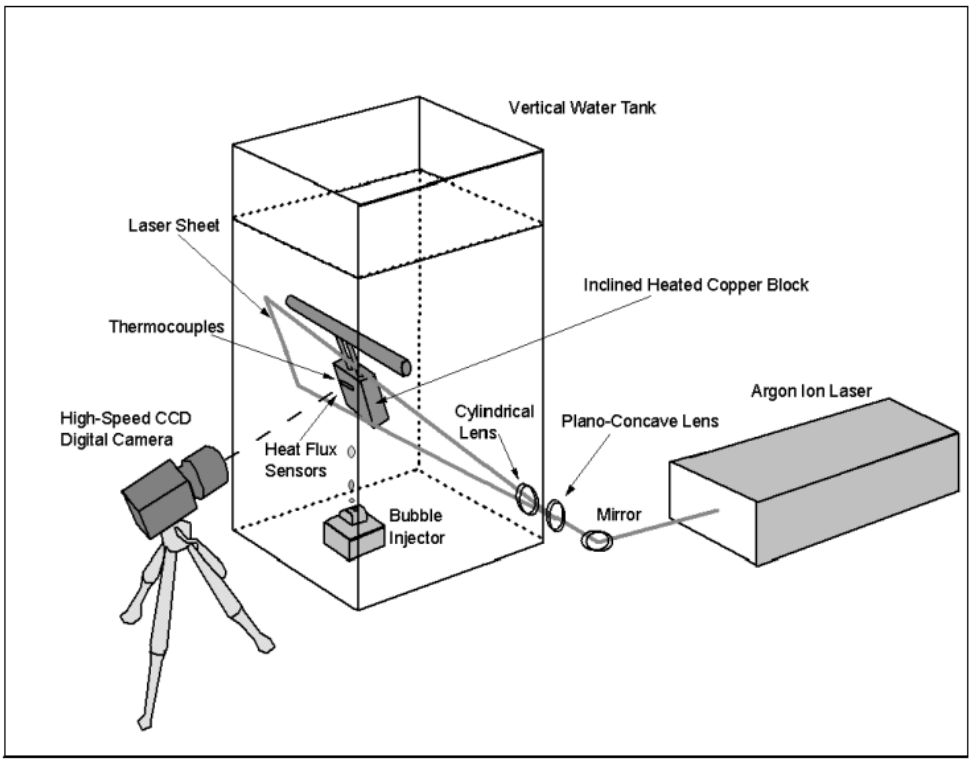

Figure 2 Schematic drawing of the experimental set-up including the water tank, the instrumented block, the PIV set-up and an inclined block.

2.2 Flow characterisation

The flow characterisation part of this experimental study aimed to provide a velocity map of the unsteady flow structure in the vicinity of the hot film rather than a point velocity measurement. The basis for this is that, if the

study is limited to a two-dimensional (2D) investigation of a three-dimensional (3D) random flow problem, it is necessary to resolve the flow structure in both time and space before attempting to characterise the flow conditions locally. For example, if an out-of-plane velocity component due to a vortex structure is not detected at one particular point by a 2D method, the in-plane influence of the vortex on the surrounding flow should be shown if a whole field measurement technique is used, thus giving some indication of the flow structure.

As mentioned in the previous section, the flow field is recorded by a high-speed camera and analysed by a Particle Image Velocimetry method capable of resolving the flow in both space and time. A 75mm lens is used with the Dalsa camera to image a 19.5mm square section of the fluid domain, parallel to the block surface. The 1mm thick laser sheet used to illuminate the flow field, approximately three millimetres from the block, is generated using a combination of a plano-concave lens of –50mm focal distance and a cylindrical lens of 150mm focal distance. A frame rate of 490Hz under continuous illumination was shown to be sufficient to resolve the highest velocities generated. The x and y velocity components (horizontal and vertical components in the case of a vertical block) are computed in the plane of the laser sheet using windowing cross correlation of successive images: The spatial displacements are obtained within each of the 32x32pixel or 2.4x2.4mm^2 interrogation windows used to discretise the image, by detecting in-plane spatial displacement of seeding particle patterns assumed to be preserved between successive frames. The velocity computed for each interrogation window, thus characterises the bulk displacement of the fluid volume contained in the windows. By repeating the computation over an 8x8 pixel mesh, the velocity map is discretised at 0.6mm intervals in both x and y directions. Two further numerical techniques are implemented to 'improve' the velocity plots. First, a 3x3 kernel median filter is applied to the two component velocity matrices to discard estimates showing abrupt changes in velocity magnitude. The mean velocity augmented by three times the standard deviation is chosen here as cut-off velocity. Second, because of the limited power of the laser source a perfectly uniform particle distribution could not be achieved by increasing the particle concentration. An interpolation technique is implemented at the post processing stage to estimate the velocity in drop out regions. The DPIV code was adapted from a freeware (URAPIV) written in MATLAB by Liberson and Gurka (1999). Additional image processing is also performed to locate the position of the bubble. The illumination of the bubble interface exposed to the laser sheet may be easily detected and is used here to locate the right hand side boundary of the bubble, while a direct inspection of the flow images gives complementary information on the bubble size and velocity.

Sample results, obtained with a 4mm diameter bubble, are shown in Figure 3 at three successive stages of the analysis. The velocity plots are shown along with the right hand side of the bubble edge appearing as a closed thick solid line contour and the hot film shown as a horizontally marked segment . The position of the hot film indicates the location where heat transfer measurements are performed. The velocity vectors are scaled to avoid overlapping between neighbouring cells. They do not, therefore, give the true magnitude of velocity but provide instead a qualitative description of the flow structure as calculated by the PIV method. A brief inspection of a series of velocity plots clearly shows that the main difficulty, from the point of view of image analysis, arises from the presence of the bubble, which is seen as a large particle spanning several interrogation windows. If the shape and orientation of the portion of the bubble interface, which reflects the light, is steady the results appear to be consistent and accurate, giving a good indication of the bubble velocity. However, if shape oscillations occur or if the bubble position in relation to the light plane changes, errors may result from sudden shifts in the light diffraction patterns. Shadow zones towards the bubble centroid may also alter the relevance of the results in this region. Similarly, due to experimental constraint, no velocity measurement is possible in the shadow zone of the bubble, ie. on the left hand side of the bubble for the present configuration. Besides if the bubble is slightly out of plane with the laser sheet, it is still detected by the PIV analysis, giving velocity estimates, which clearly do not reflect the velocity in the plane of interest. As a general rule, care should be taken in the analysis of velocity estimates in the immediate vicinity of the bubble interface. In the bubble wake as well as in the fluid region surrounding the bubble, the velocity distributions, however, appear to be consistent in both time and space. The two first velocity plots of Figure 3, show that the interpolation does not alter the general structure of the wake. A comparison of the two successive velocity maps, shown as the two last plots of Figure 3, also supports the repeatability of the results. The velocity plots of Figure 4, illustrate the level of resolution attained several tens of milliseconds after the bubble passage. If the calculations fail to reproduce small vortices (diameter of the order of 1.5mm), which are present in the flow at the times considered here, they clearly outline the flow patterns, which span several interrogation windows. As it is these larger scale flow structures, which are used to characterise the wake of a bubble for the purpose of the present heat transfer analysis, the method was deemed suitable for the study.

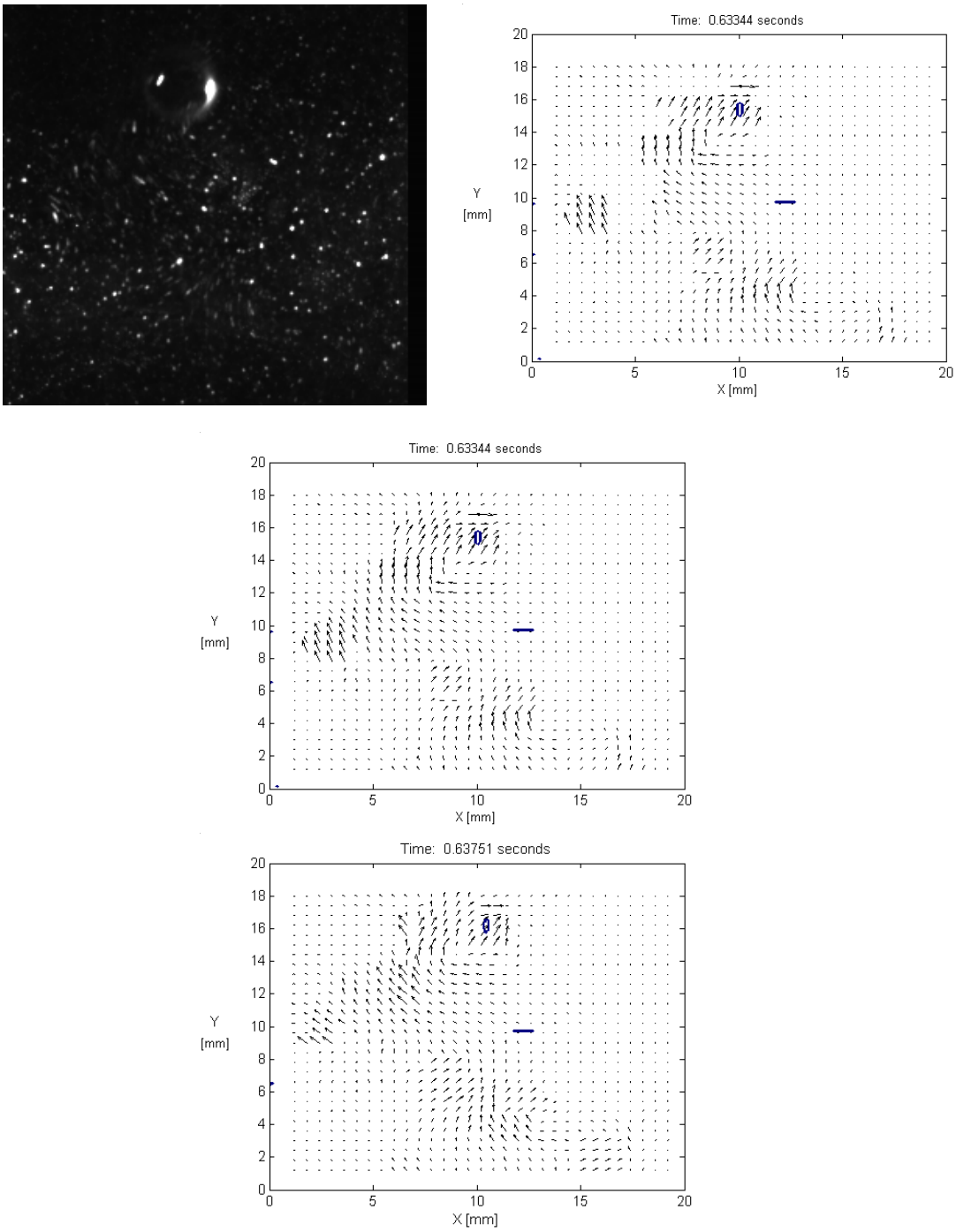

Figure 3 The high speed imaging of bubble flow in 2D plane parallel to block surface and corresponding PIV measurements shown with contour plot of right hand side of bubble interface and hot film position. Top left image frame with bubble sliding along plane as recorded from CCD camera. Top right: Velocity vector distribution from PIV before velocity interpolation over drop out regions . Bottom left: Velocity vector distribution from PIV with velocity interpolation. Bottom right: Velocity vector distribution and velocity amplitude contour plot from PIV.

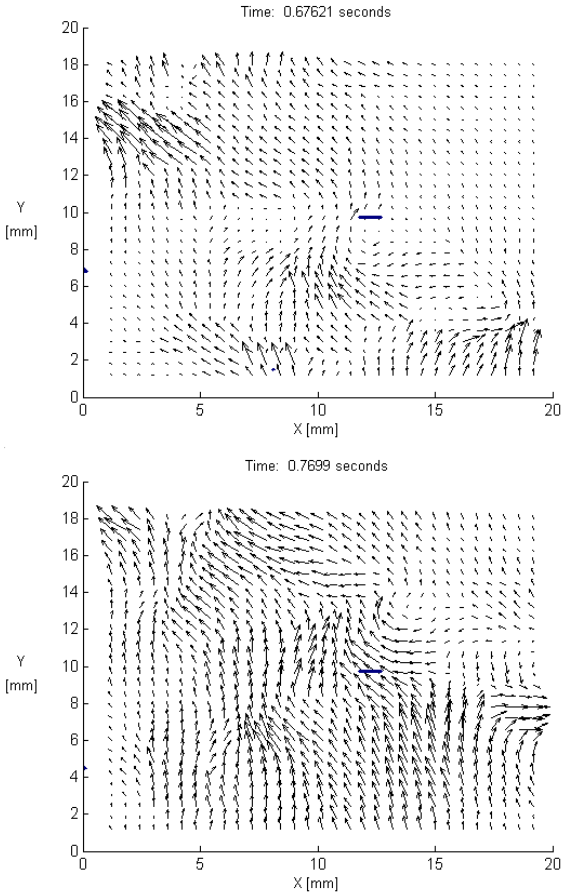

Figure 4 Velocity map after passage of 4mm diameter bubble at two different times.

2.3 Heat transfer evaluation

The hot film sensor, operated in a constant temperature mode, was selected for time varying analysis of local heat transfer because of its natural fast response time. The operating principle involves maintaining the hot film at a constant temperature and using the power consumed by the hot film as a measure of heat loss from the solid surface. The active temperature control is performed by the CTA 54T30 Dantec Wheatstone bridge with a ratio of 1 to 20. The bridge output voltage corresponds to the time varying voltage applied across the hot film. If the sensor's total electrical resistance is also known, this voltage can, therefore, be used as a direct measure of the dissipated power. The hot film resistance, which is temperature dependent and hence a function of the intensity of the current flowing through it, is controlled by the CTA bridge by setting the passive arm resistance. Under the present test conditions, outlined in the next section, the hot film is heated to 60ºC to ensure that the surrounding fluid and solid temperature is always lower than the film temperature and hence that power is always dissipated by the film giving a positive bridge output voltage. The analysis then relies on the three following assumptions:

(i) The power dissipated by the bridge is assumed to be entirely due to heat loss from the hot film to its surroundings,

(ii) The heat transfer from the hot film, when the block is heated, is modelled as a combination of convective and conductive cooling. The conductive cooling takes account of the heat loss from the film to the block through the sensor substrate and the adhesive layer. The convective cooling corresponds to the heat loss from the hot film to the flowing fluid.

(iii) By assuming that the rate of energy flux through the block surface and through the hot film are in equilibrium, the convective heat loss can be derived from the above, providing that surface area of the hot film is known. The physical size is corrected to account for edge effects and deduced by equating the heat flux obtained by this method to the Microfoil heat flux sensor measurements. This calibration method relies on the accuracy of the calibration provided with the Microfoil sensor as

well as on the accuracy of the function relating the hot film resistance to its temperature, which is provided by the hotfilm sensor manufacturer. It also assumes that the effective surface area of the hot film sensor does not vary significantly with the flow conditions.

The rate of convective heat flux q_{conv} can then be derived from the rate of heat flux dissipated by the hot film q_{diss} and the rate of conductive heat flux q_{cond}, from Equation 1.

$$q_{diss} = \frac{V^2 R_P}{A_{eff}\left(R_P + R_{Ta}\right)^2} = q_{cond} + q_{conv} = q_{conv} + \left(\frac{\delta_{Polyimide}}{k_{Polyimide}} + \frac{\delta_{adhesive}}{k_{adhesive}} \right)^{-1} \left(T_{film} - T_{block}\right) \qquad \text{Equation 1}$$

where V is the CTA bridge output voltage, A_{eff} is the effective surface area of the hot film, R_p is the hot film sensor resistance, R_{Ta} is the top resistance of the active arm of the CTA bridge and T_{film} and T_{block} represent the temperatures of the hotfilm and the block surface respectively. The relevant properties and dimensions of the hotfilm substrate and adhesive are listed in Table 1.

Table 1 Hot film sensor arrangement: material properties and layout

Material	Coefficient of conductivity, k	Layer thickness, δ
Polyimide	0.29 W/mK	0.05mm
Adhesive	0.2 W/mK	0.1mm

2.4 Experimental procedure

The experimental procedure may be summarised as follows. The copper block is set in its vertical position and the bubble injection apparatus is positioned to ensure that the free rising bubble oscillates along the block and passes within 10mm of the hot film. The bulk water temperature is brought to within ±0.3ºC of 20ºC and the bulk water is left undisturbed until a steady state is reached. The block internal heaters are then switched on by increasing the power supply to 130V at which stage the heating power reaches 318.5W. A single bubble is released after a minimum of 5 minutes when the temperature reading from the block internal thermocouple stabilises. The temperature difference between the block surface and the bulk water then approaches 30ºC. If the distance between the hot film and the bottom edge of the block is taken as reference, the corresponding Rayleigh number is of the order of 2.3×10^8 which is lower than the critical value that characterises transition to turbulent free convection flow from a vertical plate.

Data acquisition from the three thermocouples and the hot film sensor is triggered simultaneously to the camera recording as the bubble approaches the lower edge of the block. Sampling is performed at 490Hz and interrupted after 2300 samples have been recorded. The procedure is repeated until the bubble is seen, from the high speed imaging, to have passed once in front of the hot film and once on its side but still within 10mm.

3 BUBBLE FLOW CHARACTERISTICS

The results discussed here refer to a series of tests involving bubble diameters ranging from 3.5 to 4.5mm. The diameter is defined here as the length of the bubble projected on the major axis of the ellipsoid. Within this diameter range, air bubbles in water take an oblate ellipsoidal shape, with the minor axis oscillating around the vertical direction. Two types of trajectories exist for such bubbles under free rise condition. A zigzagging motion, which describes transversal oscillations occurring in the vertical plane and perpendicularly to the bubble rise, is one possibility. A spiralling rise may also occur in either clockwise or counter-clockwise directions. The motion characteristics are known to depend on the bubble diameter and the liquid properties. It may be summarised from Fan and Tsuchiya (1990) that bubbles of equivalent diameters larger than 3mm are most likely to oscillate following a zigzag path when the water contains impurities even at a very low concentration.

The impact of vortex shedding on the trajectory of free rising bubbles has been well documented (see Clift et al.,1978 or Fan and Tsuchiya, 1990 for reviews), although detailed descriptions of the complex coupled phenomena involved are still scarce. A recent study of zigzagging and spiralling air bubbles in water, which combines high-speed imaging and PIV measurements by Brücker (1999) is an exception to this. It proposes a qualitative model of the entire wake from the freely rising bubble. The model, which reconstructs the formation and shedding of three dimensional vortices from a 6mm diameter bubble, agrees well with the flow visualisation published by Lunde and Perkins (1995) as reproduced in Figure 5. The structure of the shed vortex, sketched by

Brücker(1995), is described as a so-called hairpin vortex composed of two streamwise vortex filaments or 'legs' connected by two vortex 'heads' to form a closed contour. From this model, the zigzaging motion can be explained by the shedding of the hairpin vortex head as the interaction of the resulting circulation around the bubble periphery with the free stream velocity generates a transversal lift. The periodic shedding of vortices of opposite circulation on opposite sides of the bubble equatorial plan explains the oscillatory characteristics of the rise path. Brücker also suggested that this self-induction effect causes the hairpin to curve inward below the bubble, thus limiting the transversal spreading of the wake. An ideal reproduction of this pattern leads to a wake extending downward with successive hairpin vortices of opposite circulation forming the vortex chain shown on Figure 6. The flow visualisation of Lunde and Perkins, however, suggests that vortices quickly evolve to generate a complex flow structure as non-uniform self-induction effects distort the hairpin vortex unevenly.

The qualitative analysis of Brücker's model can be carried further in the current investigation by assuming the bubble to rise along a flat surface. The dynamics of the bubble and the structure of its wake will then clearly depend on the interaction between the bubble and the solid boundary. If the flat surface is vertical, the interaction will be dependant on the angle between the surface and the bubble's zizaging plane as well as the distance separating the bubble from the surface. Inclined blocks can also be anticipated to have a stronger influence on the bubble dynamics and its path. Following impact on such an inclined surface, the motion of the bubble can be shown to involve a bouncing component and a sliding motion. The predominance of either component is then dependant on the flow conditions, the degree of inclination of the surface and the delay from impact. By slowing down the bubble the interaction is likely to reduce the generation of vorticity at the bubble interface and affect the shedding of vortices and their structures.

For both inclined and vertical walls, the bubble passage is followed by the wake. As the vortices shed, before and after impact, are convected upward, the flow conditions along the surface will experience strong variation in both magnitude and direction. For example, if an ideal hairpin vortex impacts on an inclined surface with its plane of symmetry perpendicular to the surface, the flow at the block surface should be influenced by both streamwise and transversal vortices: The top and bottom heads of the hairpin vortex should induce vertical flow components of opposite signs. As the hairpin is convected upward along a distance ranging from the top head to the bottom head, the vortex induced flow components tilt successively towards and away from the horizontal direction.

The above analysis is clearly idealised since the shape and strength of the legs of the vortex hairpin are unsteady and evolve following complex and largely unpredictable patterns. It is, however, the interaction between this wake as well as the aloft and side regions of the bubble boundary flow with the free convection flow from the heated block, which affects the local heat transfer from the block surface. The schematic description deduced from Brücker's model thus provides a qualitative understanding particularly useful for the interpretation of experimental results presented hereafter.

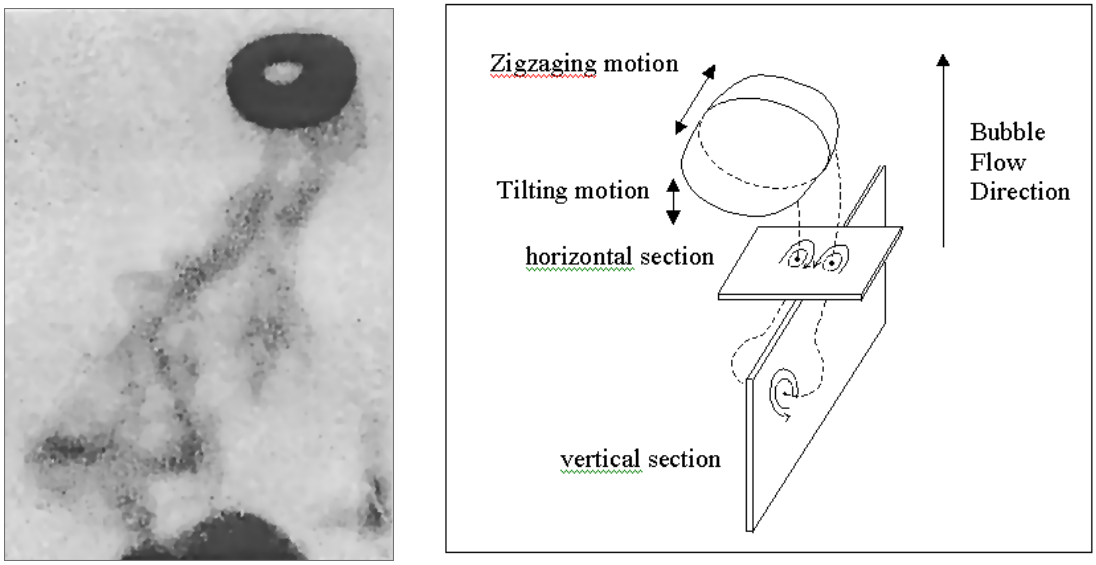

Figure 5 Wake of free rising ellipsoidal air bubble zigzaging in water at Re ~ 1500. Left: Flow visualisation from Lunde and Perkins (1995). Right: Schematic Interpretation following Brücker (1999).

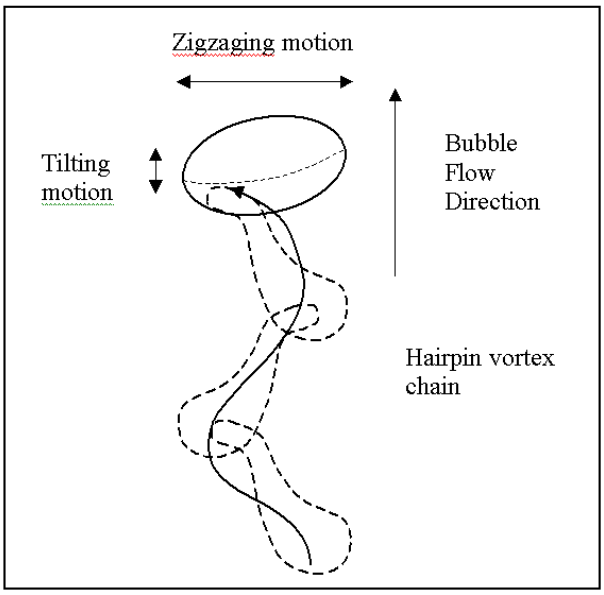

Figure 6 Schematic diagram of vortex chain formed by shedding of hairpin vortices by free rising ellipsoidal bubble. Interpretation from Brücker (1999).

4 RESULTS AND DISCUSSION

Results from a single test are discussed in this section. The aim is to clarify the main convective cooling effects, which characterise the interaction of a single rising bubble with the free convection flow from a heated vertical flat surface. The test selected involves a 4mm diameter bubble, which slides about 5mm to the left of the hot film.

Two preliminary remarks can be made from a direct inspection of the sequence of images recorded. An average bubble vertical speed of the order of 222mm/s is measured over the image area. Similar rising velocities were measured from the four other tests completed with a similar bubble size. The close agreement with existing correlations of the terminal velocity of free rising bubbles (see for example Fan and Tsuchiya, 1990), indicates that the wall effect has a limited impact as far as the bubble rising velocity is concerned. A zigzagging motion is also seen to persist suggesting that wall effects do not suppress the shedding of vortices. The bubble effect on the flow along the block surface can, therefore, be anticipated to induce swirl in both the near wake and the far wake.

A more precise quantitative and qualitative analysis is achieved by comparing instantaneous measurements of heat flux and temperature differences between the block surface and the adjacent fluid (ΔT) with flow velocity measurements and referring to a conceptual model based on Newton's law of cooling. The idea is to separate out the effects of changes in temperature gradients from the effects of variation in the flow conditions. A heat transfer coefficient h is used to define the local heat flux $q = h.\Delta T$. The fluid temperature is obtained from the external surface thermocouple while the block surface temperature is given by the internal thermocouple. It must be noted that the external thermocouple does not give the true fluid temperature at the surface, as it is influenced by convection from the fluid domain and conduction from the block through a thin silicon layer. As conduction should only depend on temperature whereas convection also varies with the flow conditions, their relative importance may vary and affect the temperature reading. Estimates of heat transfer resistance and temperature differences indicate that conduction may account for a non negligible part of the heating of the thermocouple junction, especially when the convective heat transfer is at its lowest before the passage of the bubble. The result is an overestimation of ΔT (assumed to represent the temperature difference between the block surface and the adjacent fluid). Also this overestimation may be more pronounced before the bubble passage than when the wake passes the measurement point, as in the latter case the importance of convective cooling should increase due to higher flow velocity and fluid mixing.

The temperature and heat flux time traces are compared independently with the flow velocity magnitude averaged along the hot film as well as against each other on Figure 7. This information is complemented by the selection of velocity maps shown on Figure 8. These results are reviewed and analysed below in chronological order, starting from the undisturbed free convection state and ending more than 4s later at a stage when the

effect of the wake is still significant. Two main stages are identified and used to characterise the influence of the bubble passage.

First, until the 0.7s time reference, the bubble effect on heat transfer appears to be exclusively due to its impact on flow conditions as no temperature changes are recorded from either surface thermocouples. The predominant heat transfer phenomenon is then linked to the ability of the working fluid to transport heat away from the block surface purely under the influence of increased volume flux. Five main observations are made from an analysis of this initial stage:

(i) The free convection flow is characterised by a relatively uniform flow slightly inclined towards the edge of the block, which is about 13mm from the end of the hot film. The steady state flow velocity is then of the order of 7.8mm/s. As the fluid is displaced ahead and on the side of the rising bubble, the fluid velocity increases and the flow direction is altered. The effect on the heat transfer is small but non negligible with an increase of about 15% being recorded for a 40% rise in the flow velocity.

(ii) This upward trend reverts as soon as the fluid velocity reduces. The cause is shown in Figure 8.c to be a swirl generated on the right hand side of the bubble. Its intensity is moderate but sufficient to halve the upward free convection flow. The drop in heat flux is of the order of 8%.

(iii) The heat transfer appears to respond with a delay to the increase in flow velocity after the next flow reversal caused by the wake. Similar observations are made at a later stage of the flow and may be due to the fact that velocities are measured a certain distance from block surface and that the flow interaction with the boundary layer is clearly not instantaneous.

(iv) Comparing the free convection heat transfer with its value at 0.7s just before ΔT starts changing, gives an increase of about 43% for a 300% rise in flow velocity. A possible reason for this relatively weak dependence is that the flow is most likely laminar since both the Rayleigh and Reynolds numbers are well below their transition values.

(v) It is interesting to note that the observed pattern of a minor peak in heat transfer followed by a sharper rise always occurs regardless of the position of the side vortices in relation to the measurement point, providing that the near wake does reach the sensor. This is also the case when the bubble passes in front of the sensor but some distance from the surface.

Second, from the time the fluid layer temperature starts fluctuating, the heat transfer results from the combined effects of temperature gradients and flow conditions. Four main conclusions are drawn from this second phase:

(i) The delay between the bubble passage and the onset of temperature change recorded by the external thermocouple is relatively long. Results indicate that the bubble drags colder fluid from the bulk water region in its near wake and that the colder fluid region is well localised within a relatively narrow 'pocket'. The delay therefore depends on the trajectory of the wake and the trapped cold water region, again, in relation to the measurement point. Figure 8.e to g, which refer to the flow before and after 0.7s, shows a fluid region with velocities in its core reaching 100mm/s but which convects at the average velocity of the wake. This suggests the presence of a vortex structure whose passage in front of the hot film coincides with the onset of temperature changes.

(ii) The peak in heat transfer is reached slightly after the peak in fluid velocity and before the maximum temperature difference. If Newton's model is considered, the results would indicate a 370% rise in the heat transfer coefficient. This sharp rise by comparison with the previous 42% value measured at 0.7s, occurs in spite of the moderate growth in the velocity magnitude. It may be overestimated due to the overestimation of ΔT during free convection, but also probably reflects three dimensional flow phenomena, which cannot be fully accounted for by the present 2D PIV technique. In any case, the strong curvatures in the streamlines, shown on Figure 7.h around the hotfilm, does indicate a strong fluid mixing, most likely linked to three dimensional flow patterns and clearly conducive to inducing large heat fluxes.

(iii) Another striking result is the close correlation between the temperature and heat transfer fluctuations observed after the first peak and shown on the bottom part of Figure 7. As the velocity reduces in the further wake, it is tempting to conclude that temperature gradients become the dominant factor governing heat transfer. One example is the passage of a cooler fluid volume from 2.6s to 3.4s, which triggers a heat flux oscillation closely correlated to the temperature oscillation. This pattern is shown to follow an increase in fluid velocity but to reduce relatively quickly although the faster flow persists. Results at this stage are, however, not entirely consistent as the relatively large temperature differences and in some cases large flow velocities, by comparison with their free convection values, should lead to higher heat flux values. This may be caused, as discussed previously, by an overestimation of the temperature difference before the bubble passage.

(iv) From the point of view of the wake interaction with the block surface, another interesting conclusion can be drawn from the last fluctuation shown between 2.6s and 4.4s on the graphs of Figure 7. The first

aspect, which was highlighted in the latter point, is the close correlation between the onset of velocity increase and temperature drop. Figure 8.i and .j shows that this is associated with a region of transverse flow as could be caused by the zigzagging motion of the bubble and associated oscillations in its wake but also by a streamwise vortex. For example, if the leg of a vortex hairpin is assumed to be the cause, as Brücker's model would suggest, it should be followed by the head of the hairpin vortex. The flow direction should then show a gradual shift towards the vertical direction providing that the vortex axis is parallel to the block surface. Figure 8.k indicates that this may be indeed occurring. Another fact that supports these conjectures, or at least an explanation of the observed flow pattern by an out of plane vortex, is the fact that this fluid region is displaced at half the instantaneous velocity measured in its core, suggesting the presence of a vortex (see Figure 8.l). Also Figure 8.l shows a velocity plot, which is characteristic of an out of plane vortex with straight flow at the core and even curvatures along the edges. Such a vortex can be expected to carry cold fluid from the bulk water volume thus causing the observed temperature fluctuations.

5 CONCLUSION

Heat transfer from a vertical flat surface heated to 50ºC and immersed in water at 20ºC has been investigated under the influence of single rising ellipsoidal bubbles. Velocity estimates obtained from PIV measurements were used along with heat flux and temperature measurements to characterise the heat transfer and fluid flow processes involved. Local as well as whole field velocity measurements proved to be essential in improving the understanding of the bubble wake and, in turn, its influence on heat transfer. Two essential mechanism were identified: First the heat transfer coefficient was found to respond closely to changes in the flow velocity. Vortices present in the near wake, for example, have been shown to successively enhance and hinder heat transfer as they assist and oppose the free convection flow. Second, fluctuations in the external fluid temperature due to bubble agitation have been linked to large simultaneous oscillations in heat transfer: Vortices, which are shed by the bubble and convected by the wake induce temperature fluctuations by bringing colder fluid into contact with the block surface. The largest heat flux occurs when both effects are combined, that is shortly after the bubble passage as the flow velocity is still much higher than its free convection value and as the first out of plane vortex drags cold fluid past the heat flux sensor. A five-fold increase was observed, for example, from the test results used to illustrate the present analysis.

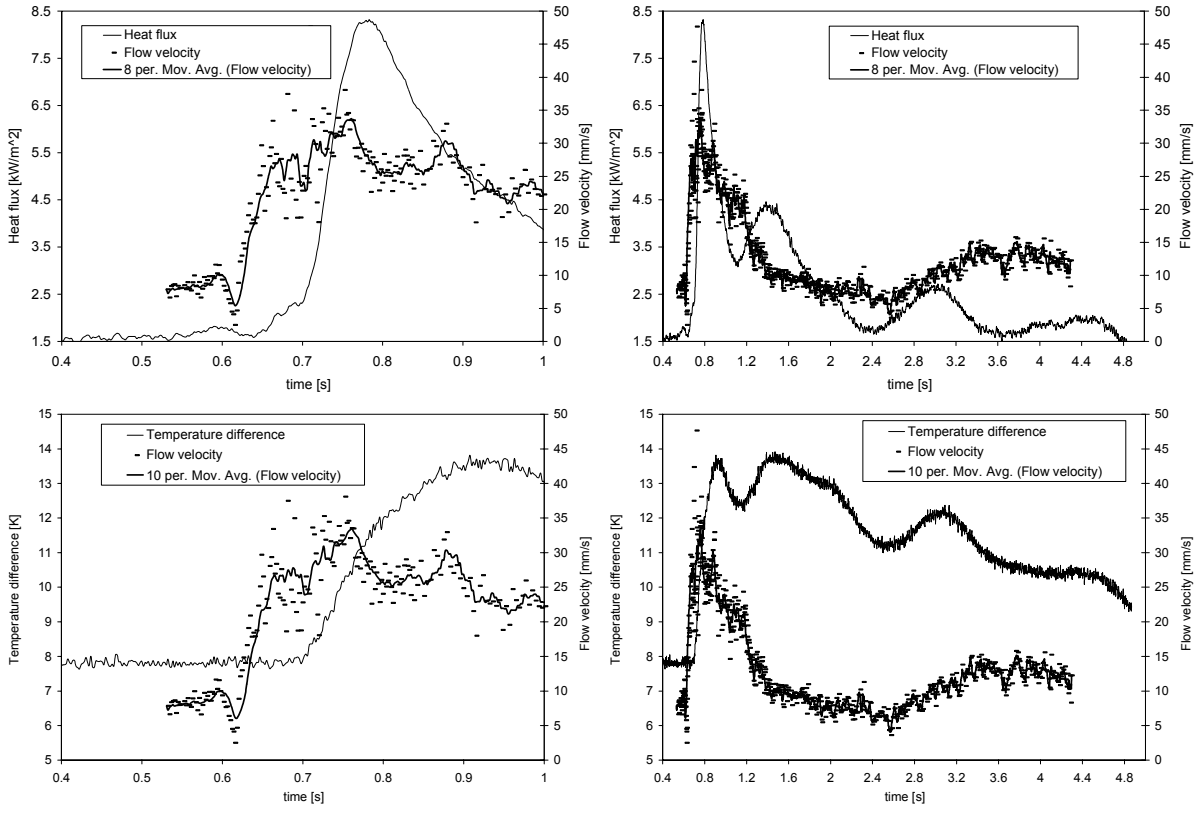

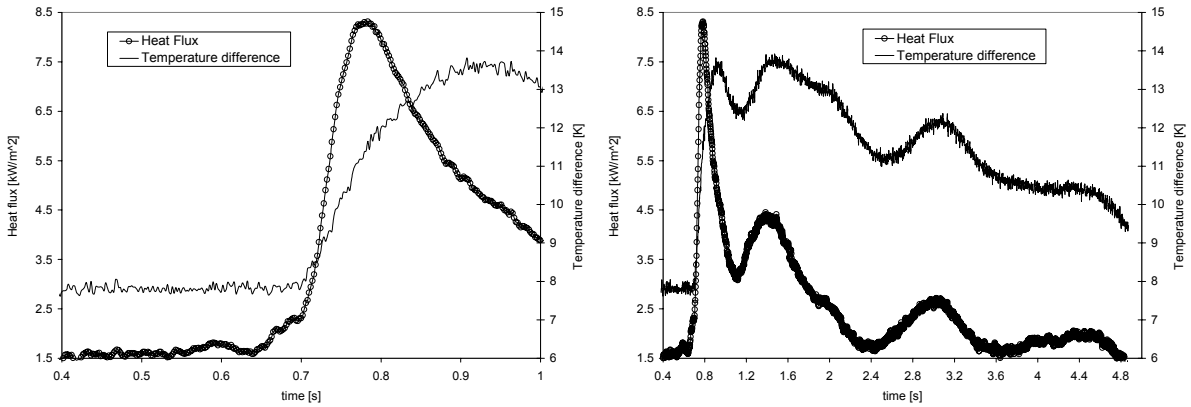

Figure 7 Variations in local heat flux and temperature gradient at the block surface before and after the passage of single bubble. Top: Comparison of heat flux with flow velocity at hot film for two different time scales. Middle: Comparison of temperature gradients with flow velocity at hot film for two different time scales. Bottom: Comparison of temperature gradients with local heat flux.

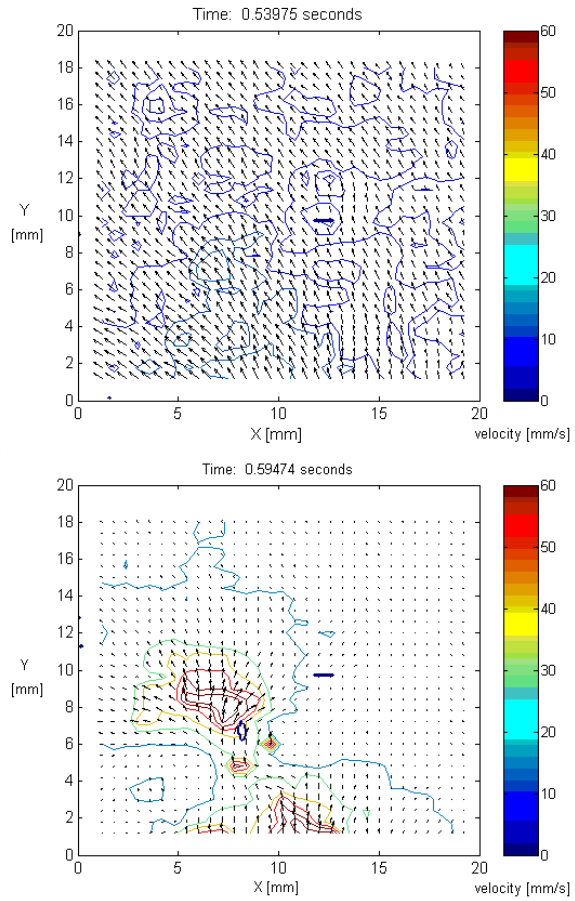

(a) (b)

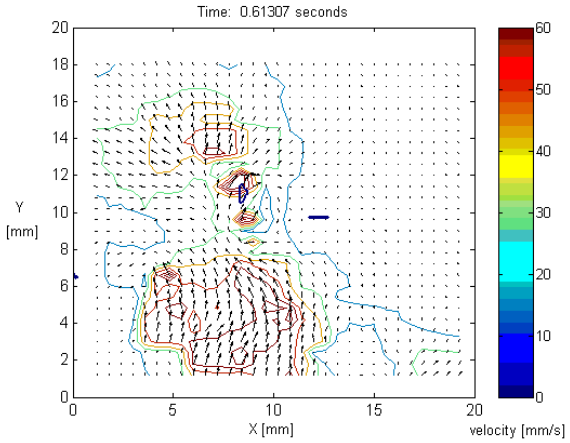
Time: 0.61307 seconds
Y [mm]
X [mm]
velocity [mm/s]

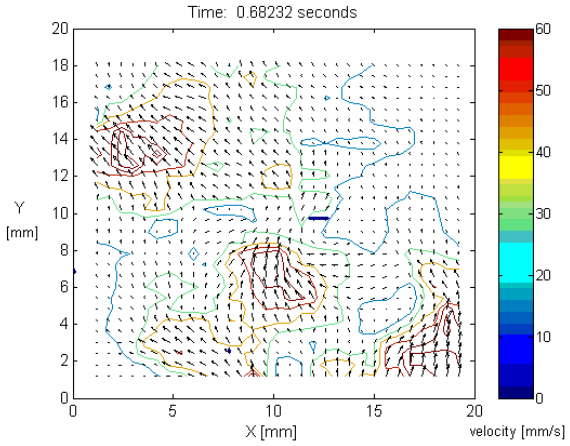
Time: 0.68232 seconds
Y [mm]
X [mm]
velocity [mm/s]

(c)

(d)

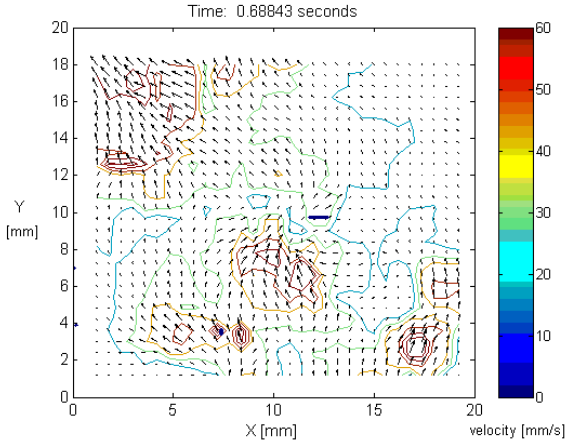
Time: 0.68843 seconds
Y [mm]
X [mm]
velocity [mm/s]

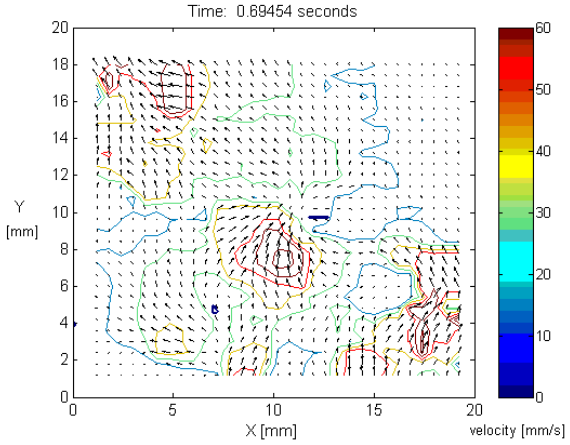
Time: 0.69454 seconds
Y [mm]
X [mm]
velocity [mm/s]

(e)

(f)

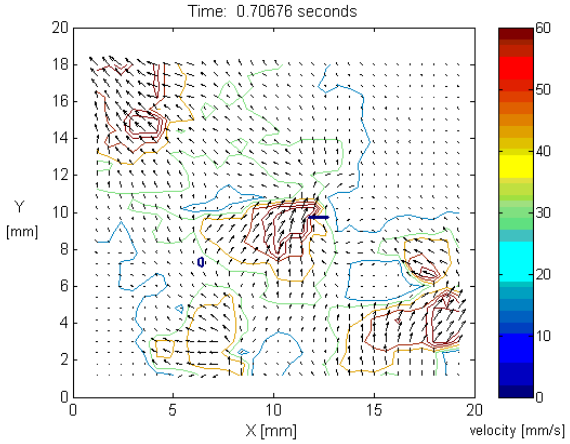
Time: 0.70676 seconds
Y [mm]
X [mm]
velocity [mm/s]

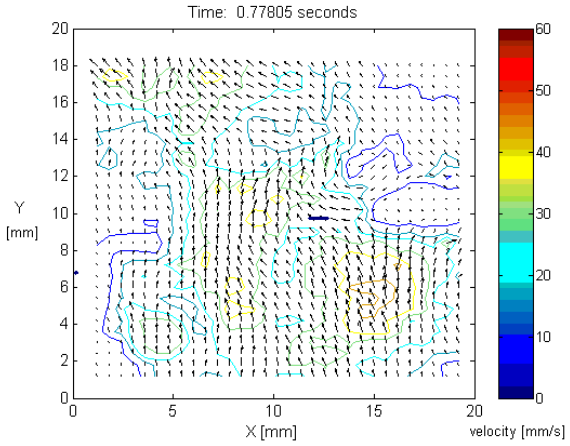
Time: 0.77805 seconds
Y [mm]
X [mm]
velocity [mm/s]

(g) (h)

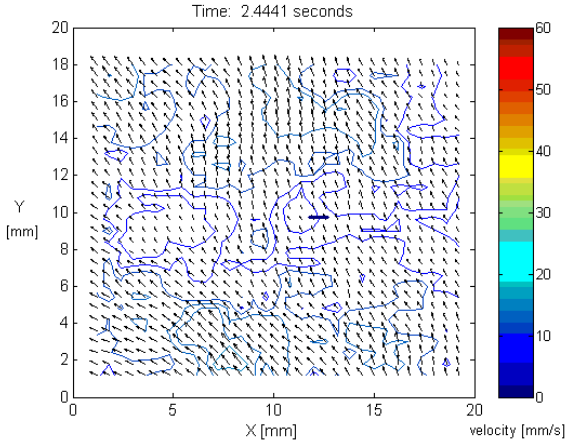
Time: 2.4441 seconds
Y [mm]
X [mm]
velocity [mm/s]

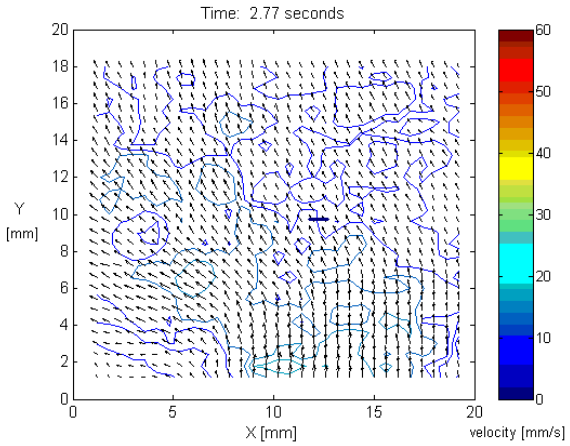
Time: 2.77 seconds
Y [mm]
X [mm]
velocity [mm/s]

(i) (j)

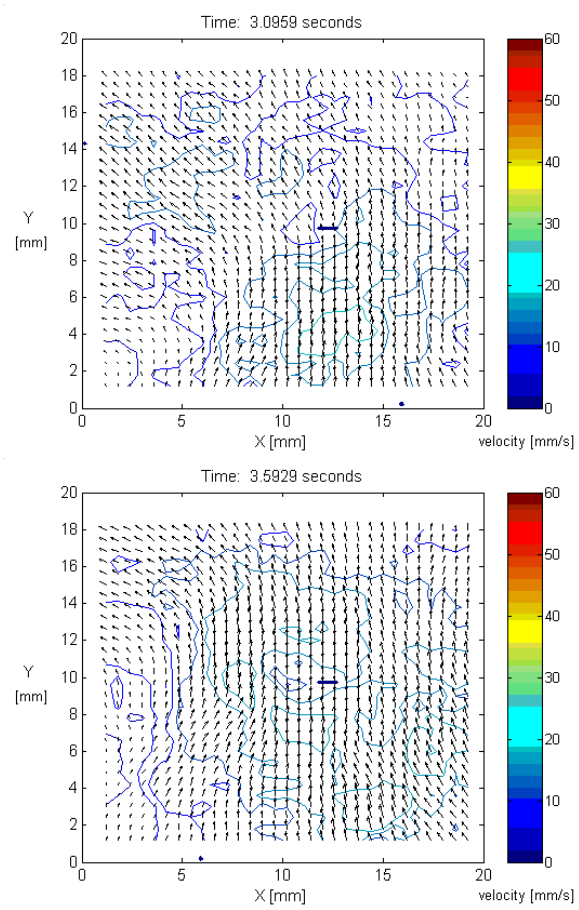

(k) (l)

Figure 8 Flow velocity plots from PIV measurements shown with velocity vectors automatically scaled to avoid overlapping, velocity contour plot showing true velocity amplitude in mm/s, a contour plot of the right hand side of the bubble interface and a straight line indicating the hot film position and dimension.

ACKNOWLEDGEMENTS

The authors gratefully acknowledge the financial support of Enterprise Ireland under its basic research programme, grant number SC/2000/235, and of the European Union under a Development Host Fellowship scheme.

REFERENCES

C. Brücker, "Structure and dynamics of the wake of bubbles and its relevance for bubble interaction", 1999, Journal of American Institute of Physics, Vol.11, No. 7. pp 1781-1796.

R. Clift, J.R. Grace and M.E. Weber, "Bubbles, Drops and Particles", 1978, Academic Press Pub.

L.-S. Fan and K. Tsuchiya, "Bubble wake and liquid-solid suspensions", 1990, Butterworth Heinmann Series in Chemical Engineering.

Forster, K.and Grief, R., "Heat transfer to a boiling liquid – mechanism and correlations", 1959, Trans. ASME, J. of Heat Transfer. V. 81, pp 41-53.

A. Liberzon and R. Gurka, 1999, "http://members.tripod.com/urapiv/"

K. Lunde and R.J. Perkins, "Observations on wakes behind spheroidal bubbles and particles", 1995, Paper No. FEDSM97-3530, ASMEFED Summer Meeting Vancouver, Canada.

J.W. Scholten and D.B. Murray, 1998, "Unsteady heat transfer and velocity of a cylinder in cross flow", 1998, Int. Journal of Heat and Mass Transfer.41-10, pp1139-1156.

Yan, Y., Kenning, D. and Cornwell, K., "Sliding and Sticking vapour bubbles under inclined plane and curved surfaces", 1997, *Int. J. Refrigeration*. Vol. 20, No. 8, pp 583-591,

Youn, H.Y., Koshizuka, S. and Oka, Y., "Direct calculation of bubble growth and rise in nucleate pool boiling", 2001, International Journal of Multiphase Flow, V. 27, pp 277-298.